

pubs.acs.org/cm Article

# Leveraging Cation Exchange in InP Magic-Sized Clusters To Access Coinage Metal Phosphide Nanocrystals

Forrest W. Eagle, Samantha Harvey, Helen Larson, Autumn Abbott, Dylan M. Ladd, Kelsey R. Levine, Michael F. Toney, Daniel R. Gamelin, and Brandi M. Cossairt\*



Cite This: Chem. Mater. 2024, 36, 2888-2897



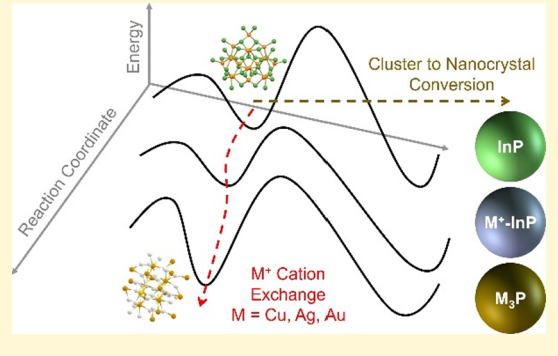
**ACCESS** 

III Metrics & More

Article Recommendations

s Supporting Information

ABSTRACT: We report the conversion of In<sub>37</sub>P<sub>20</sub> magic-sized clusters (MSCs) via cation exchange at room temperature to obtain doped InP clusters and nanocrystals, as well as Cu<sub>3-x</sub>P, Ag<sub>3-x</sub>P, and Au<sub>3-x</sub>P nanocrystals. Using a combination of spectroscopic and structural characterization, we determine that the InP clusters undergo doping with significant rearrangement of their ligand shells, but only minor changes in their cores when 1 to 5 equiv of coinage metal salt (per cluster) are added. However, when 37 equiv of coinage metal salt are added, the MSCs fully transform both compositionally and structurally into new ultrasmall coinage metal phosphide nanocrystals with complete extrusion of indium, as determined via X-ray photoelectron spectroscopy, X-ray diffraction, and pair distribution function analysis. We further document the use of these doped InP MSCs and



ultrasmall coinage metal phosphide nanocrystals for the synthesis of larger doped InP nanocrystals and a variety of coinage metal phosphide nanocrystals in the 3–15 nm size range.

# INTRODUCTION

Magic-sized clusters (MSCs) are atomically precise molecules often found as metastable intermediates in the synthesis of nanocrystals. 1-3 Due to the atomically precise nature of these clusters, their physical, electronic, and reactivity properties can be studied without complications associated with ensemble heterogeneity. In particular, MSCs serve as a unique platform for studying cation exchange. By understanding the mechanism and structural changes involved in cation exchange, synthetic chemists can rationally design new pathways to access colloidal nanomaterials that may be difficult or impossible to form by traditional bottom-up nucleation and growth.<sup>4–8</sup> Additionally, although cation exchange in III-V nanocrystals often requires high temperatures, cation exchange in MSCs can often be performed at room temperature. 9-11 While cation exchange has been widely studied in Zn- and Cd-chalcogenide MSCs, 11-17 few reports examine cation exchange in indium phosphide MSCs. 10,18 This work demonstrates the cation exchange of InP MSCs with coinage metals (Cu, Ag, and Au). Coinage metals are of interest due to the unique properties that characterize Group 11 binary compounds such as phosphides and chalcogenides, including localized surface plasmon resonances (LSPRs) and enhanced catalytic activities. Given the ion mobility associated with copper ions in inorganic lattices, <sup>19</sup> the Cu-P products are also of interest for sequential cation exchange chemistries to access multinary and high entropy materials.

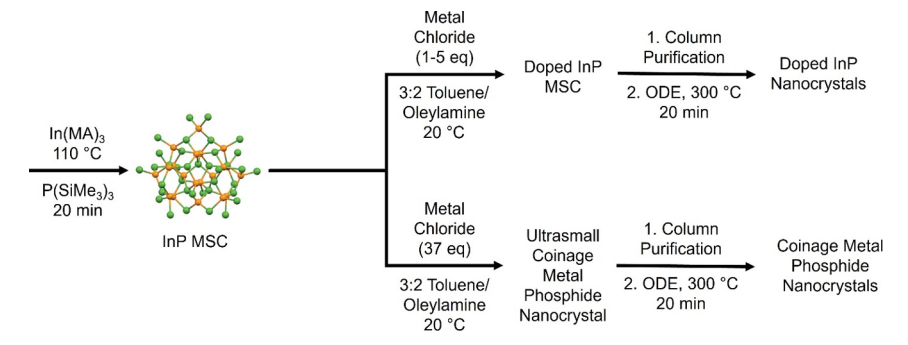
Copper phosphide has been widely studied because of the near infrared (NIR) LSPR generated in defective Cu<sub>3-x</sub>P lattices. 7,20-22 Additionally, Cu<sub>3</sub>P is notable for its efficient electrocatalysis of the hydrogen and oxygen evolution reactions, showing near-unity Faradaic efficiency during hydrogen evolution and only minor degradation after extended use. 23-26 The other coinage metal phosphides, Ag-P and Au-P, have traditionally been challenging to synthesize due to their metastability.<sup>27,28</sup> Although Ag-P compounds have been predicted to serve as excellent catalysts for CO2 reduction, accessing these materials has been synthetically challenging.<sup>29,30</sup> Homologous Ag-As and Ag-Sb compounds have been found in nature, suggesting the formation of Agpnictogen species is possible. 31-33 Au<sub>2</sub>P<sub>3</sub> nanostructures have been synthesized; 27,34 however, these syntheses require phosphorization of Au nanocrystals and often lead to large domains of unreacted Au. Additionally, although AuP has been predicted, 28 there has been no synthesis of this material at the nanoscale nor the bulk. A more complete understanding of the electronic and catalytic properties of Au-P compounds will

Received: December 20, 2023 Revised: February 16, 2024 Accepted: February 20, 2024 Published: March 5, 2024





Scheme 1. Summary of Cation Exchange Reactions of InP MSCs with Coinage Metals Forming either Doped InP MSCs or Ultrasmall Coinage Metal Phosphide Nanocrystals<sup>a</sup>



"After isolation, these products can be heated to form doped InP or coinage metal phosphide nanocrystals.

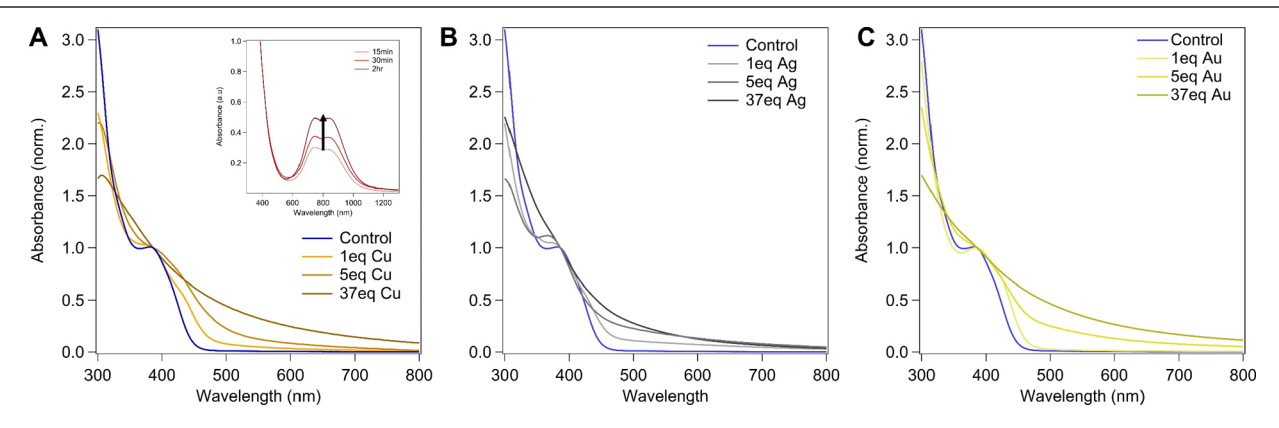


Figure 1. Absorption spectra of coinage metal-treated  $In_{37}P_{20}$  MSCs. (A) Addition of 1, 5, and 37 equiv of CuCl<sub>2</sub>. Inset: absorption spectra of clusters treated with 37 equiv of Cu followed by exposure to oxygen for the times indicated. Note that the dip at the absorption maximum is an instrumental artifact. (B) Addition of 1, 5, and 37 equiv of AgCl. (C) Addition of 1, 5, and 37 equiv of AuCl.

require the synthesis of crystalline, single-domain nanocrystals across a range of possible stoichiometries.

In this work, we demonstrate room temperature cation exchange in magic-sized InP clusters, leading to the formation of doped InP clusters or ultrasmall nanocrystals of Cu<sub>3-x</sub>P, Ag<sub>3-x</sub>P, and Au<sub>3-x</sub>P depending on the reaction stoichiometry. We further show that these small nanocrystals can grow upon heating, leading to larger nanocrystals across the coinage metal phosphide family (Scheme 1). This MSC chemistry thus provides a versatile approach to preparing, isolating, and studying coinage metal phosphide nanostructures.

# ■ RESULTS AND DISCUSSION

Given the small size of MSCs, their optical properties are susceptible to changes in lattice structure because even small perturbations can significantly impact their electronic structure. As such, UV-vis absorption spectroscopy can be used as a sensitive diagnostic tool to monitor changes in the cluster core. Upon adding low molar equivalents (1, 5 equiv) of CuCl<sub>2</sub> solubilized in a 3:2 mixture of toluene and oleylamine to the starting  $In_{37}P_{20}(O_2CC_{13}H_{27})_{51}$  cluster, we see the growth of a low-energy tail extending into the sub-bandgap region, followed by a broadening of the InP absorption band (Figure 1A). This broadening is consistent with the absorption of other Cu-doped and Cu-based nanocrystals, including Cu-CdSe and CuInS<sub>2</sub>. It is not attributed to size inhomogeneity but rather a metal-to-ligand (conduction band) charge transfer type transition involving copper-localized holes. 38-37 As such, we attribute this continuous broadening of the absorption

spectrum to the introduction of copper into the core of the MSC as opposed to exchange with the excess surface indium carboxylate Z-type ligands.<sup>38</sup> Upon adding 37 equiv of Cu (equal to the number of indium ions of the original MSC), we see a complete loss of the original absorption peak, with conversion to a broad, featureless absorption spectrum spanning the visible region. This spectrum resembles the UV-vis absorption of previously characterized Cu<sub>3-x</sub>P nanocrystals, as well as Cu<sub>2</sub>S and Cu<sub>2</sub>Se nanocrystals. <sup>20,21,39,40</sup> Furthermore, 37Cu-MSC exhibits the growth of a new feature in the near-infrared region of its absorption spectrum upon oxidation, as seen in the inset of Figure 1A. Previous reports of Cu<sub>2</sub>Se nanoclusters have also detailed the growth of a similar feature upon oxidation, attributed to a new plasmon resonance. This new feature is centered at ~800 nm, which is higher energy than the LSPRs of Cu<sub>3-x</sub>P nanocrystals, and this energy could reflect a blueshift due to quantum confinement.  $^{21,41-43}$ 

The addition of AgCl and AuCl to the  $\rm In_{37}P_{20}$  MSCs gives similar results—low equivalents of Ag and Au lead to the same spectral broadening, followed by conversion to a broad featureless absorption spectrum upon the addition of 37 equiv (Figure 1B,C). While no reports of Ag–P nanomaterials exist, this broad absorption is similar to that found in Ag<sub>2</sub>Se and Ag<sub>2</sub>S nanocrystals.  $^{44-47}$ 

We also observed similar results for  $In_{37}P_{20}$  MSCs treated with CuCl and AuCl<sub>3</sub> solubilized in toluene/oleylamine mixtures, as shown in Figure S1, indicating that the starting metal halide solution is likely reduced in situ by the oleylamine

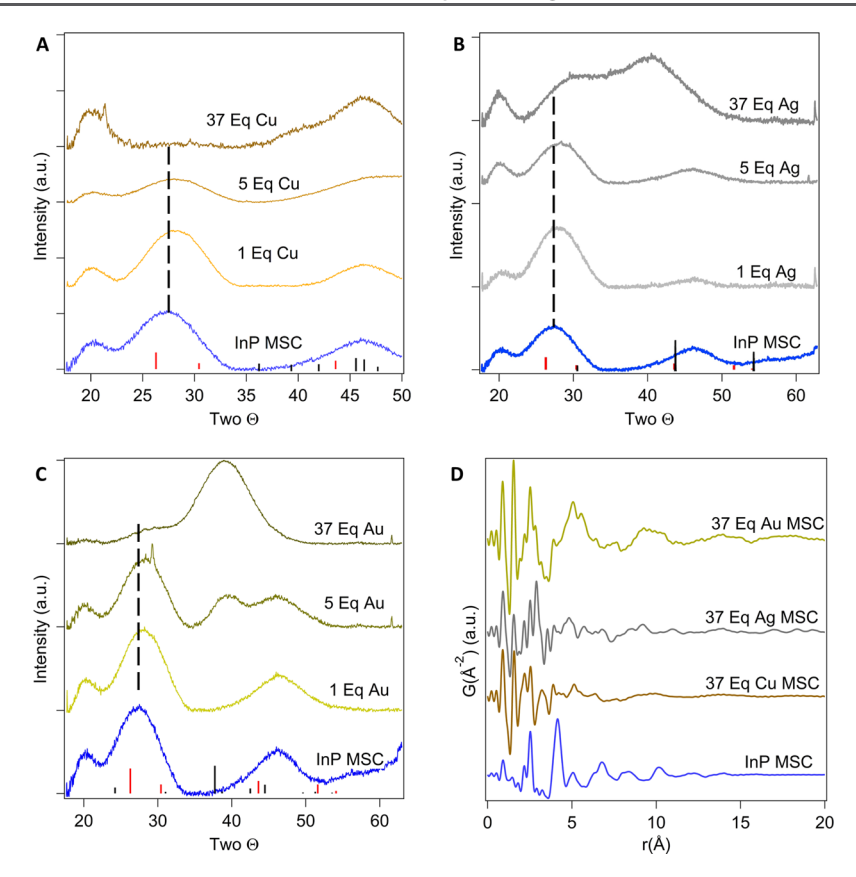


Figure 2. (A) pXRD pattern upon addition of  $CuCl_2$  to  $In_{37}P_{20}$ . Zinc blende InP is colored red and  $Cu_3P$  is shown in black. (B) pXRD pattern upon addition of AgCl to  $In_{37}P_{20}$ . Zinc blende InP is shown in red and  $Ag_3P$  is shown in black. (C) pXRD pattern upon addition of  $AuCl_3$  to  $In_{37}P_{20}$ . Zinc blende InP is shown in red and  $Au_3P$  is shown in black. (D) PDF analysis of InP MSCs and clusters treated with 37 equiv of coinage metal.

and that all products contain coinage metals in the +1oxidation state. This conclusion is confirmed by comparative X-ray photoelectron spectroscopy (XPS) analysis (Figure S2).<sup>48</sup> Interestingly, upon attempting full cation exchange with coinage metal halides solubilized by tributylphosphine, only minimal broadening in the absorbance profile is observed, suggesting hindered cation exchange when the coinage metal is introduced under these conditions (Figure S3). This result indicates that the precursor identity is important and that amines help to drive the cation exchange, consistent with the predictions of hard-soft acid-base theory. Specifically, the binding affinity of the soft tributylphosphine base for the soft Cu<sup>+</sup> (or Cu<sup>2+</sup>) is higher than it is for the relatively hard In<sup>3+</sup>, hindering exchange. In addition, tertiary phosphines do not impact the surface of the In<sub>37</sub>P<sub>20</sub> MSCs in the same manner as primary amines, which liberate indium carboxylate from the surface through a formal L-assisted Z-type ligand displacement reaction. 49,50 We believe that this interaction is essential for coinage metal coordination and subsequent exchange. We also examined the effect of the anion to further investigate the impact of precursor identity on cation exchange. Upon running the same exchange reactions with CuBr and CuI, we observed that the cation exchange was hindered relative to the chloride case (Figure S4), again consistent with predictions based on hard-soft acid-base theory. These results indicate that the anion identity can be used to tune the kinetics and extent of these exchange reactions. Previous work has shown that the addition of metal carboxylates to InP MSCs can induce cation exchange but requires much more added cation.<sup>10</sup>

The initial powder X-ray diffraction (pXRD) pattern of  $In_{37}P_{20}$  MSCs does not correspond to the zincblende phase of bulk InP. Instead, the cluster has a strained core that can be described as having a pseudowurtzite character.<sup>38</sup> Upon adding 1 and 5 equiv of  $CuCl_2$  to the MSC, we see shifting and broadening of the diffraction peaks, indicating the original lattice becomes more disordered as more Cu ions are introduced into the core (Table S1). Upon the addition of 37 equiv, the original diffraction peaks are no longer visible and instead are replaced by two prominent peaks at  $2\theta = 40$  and  $47^{\circ}$ , as seen in Figure 2A. These peaks are consistent with ultrasmall hexagonal  $Cu_3P$  nanocrystals.<sup>51</sup>

With the addition of 1 and 5 equiv of AgCl, we again see the shifting and broadening of the original  $In_{37}P_{20}$  MSC peaks characteristic of the formation of a defective lattice. Upon adding 37 equiv of AgCl, we see more drastic changes in the diffraction pattern, as shown in Figure 2B. While Cu–P compounds have routinely been synthesized and characterized, Ag–P compounds have not been successfully realized on the nanoscale despite much synthetic effort, leading to little to no literature from which to draw comparisons.  $^{29,30}$ 

Examination of the Au-doped species shows much less broadening at five equiv when compared to the Ag- and Cu-doped species; instead, the growth of a new peak centered around 40° is observed (Figure 2C). This peak corresponds with the major diffraction peak in hexagonal Au<sub>3</sub>P. Sa higher equivalents of Au are added, this new peak becomes better defined, while the peaks attributed to InP are lost. This result may suggest a highly cooperative cation exchange pathway for

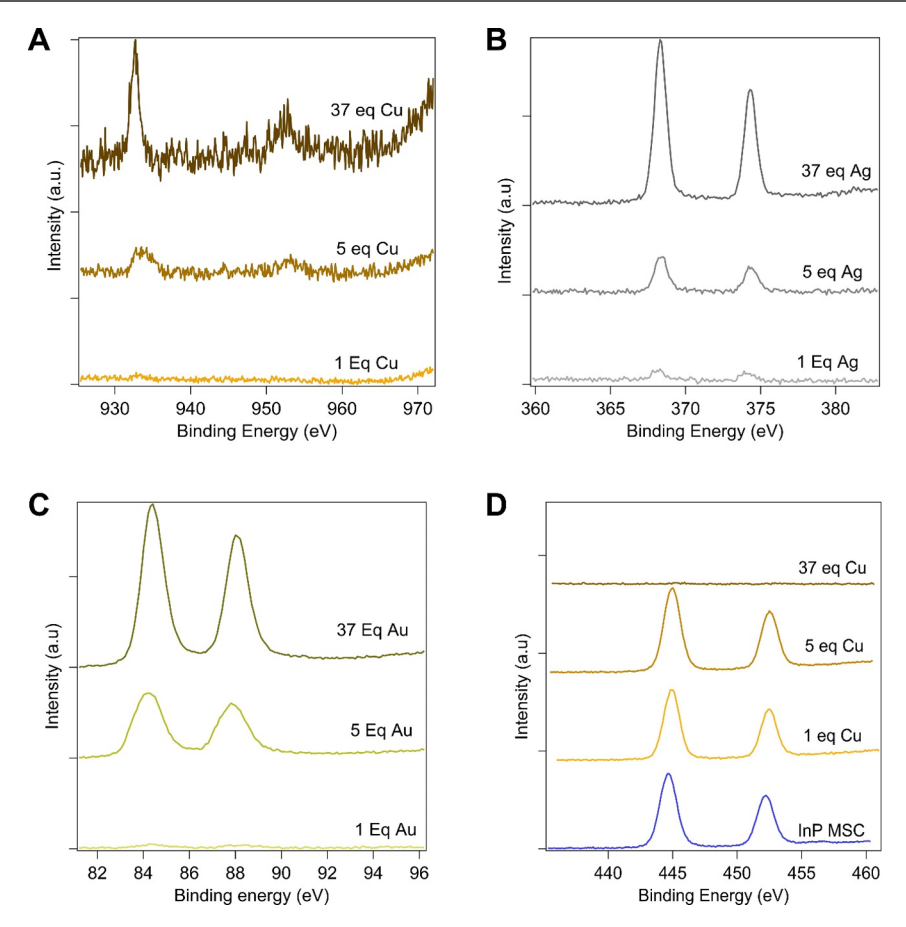


Figure 3. (A) XPS spectra of Cu 2p peaks with the addition of CuCl<sub>2</sub> to  $In_{37}P_{20}$  MSCs. (B) Ag 3d peaks upon the addition of AgCl to  $In_{37}P_{20}$  MSCs. (C) Au 4f peaks with the addition of AuCl<sub>3</sub> to  $In_{37}P_{20}$  MSCs. (D) XPS spectra of In 3d peaks upon addition of CuCl<sub>2</sub> to  $In_{37}P_{20}$  MSCs.

Au. As soon as doping reaches a critical concentration, full cation exchange is pushed to completion, similar to Cu exchange in CdSe and Ag exchange in CdS. <sup>53,54</sup> Our findings are consistent with previous experiments showing that Ag leads to a cooperative cation exchange avalanche at lower concentrations than Cu. <sup>54</sup> As the size of the Au ion is larger, the InP lattice cannot as easily rearrange around the dopant, leading to structural transformation at lower dopant concentrations. These observations support theoretical predictions that the InP MSC lattice cannot rearrange favorably around larger dopants. <sup>54,55</sup>

The broad XRD peaks observed in Figure 2A-C are consistent with ultrasmall nanocrystals, a conclusion corroborated by transmission electron microscopy (TEM) analysis showing that the average size of the fully cation-exchanged clusters is 3 nm for the Cu<sub>3-x</sub>P nanocrystals and 2 nm for the  $Ag_{3-x}P$  and  $Au_{3-x}P$  nanocrystals (Figures S5-7). The structures of these products were further investigated by pair distribution function (PDF) analysis of the 37 equiv treated samples (Figure 2D). Previous work in our group has shown the sensitivity of PDF to changes to the internal lattice of InP MSCs.<sup>2,10</sup> Most noticeably, all three exchanged samples show a loss of the prominent peak around 4.1 Å, representative of the In-In network in the original InP lattice. These data indicate that the internal lattice of the Cu-P cluster is similar to that of Cu<sub>3</sub>P nanocrystals, having major reflections at 2.25 and 2.61 Å corresponding to Cu-P and Cu-Cu distances, respectively.<sup>56</sup> Although previous PDF analysis does not exist for Ag-P or Au-P complexes, the Ag-P and Au-P clusters show new

peaks around 2.9–3.0 Å that agree well with theoretical predictions for Ag–P and Au–P bonds in  $Ag_3P$  and  $Au_3P$  (Figure S8). We note that all three clusters also show peaks at 2.2 and 2.6 Å, and it is difficult to determine if these peaks correspond to the In–O and In–P bonds of surface-bound Incarboxylate moieties or if they reflect distorted metal–metal and metal–phosphorus distances similar to those found in Cu–P. Overall, the combination of XRD, PDF, and TEM data indicate the formation of unique Cu–P, Ag–P, and Au–P clusters through these cation exchange reactions.

XPS data were collected to further resolve the composition and coordination environments of the coinage metal-treated clusters. After adding CuCl<sub>2</sub> to the In<sub>37</sub>P<sub>20</sub> MSCs, we see the growth of the expected copper 2p peaks with further increased resolution upon additional equivalents, as seen in Figure 3A. With increasing equivalents of added Cu, we also see a shift to lower binding energies by over 1 eV, with the  $2p_{3/2}$  peak reaching 932.6 eV for the 37 equiv sample. This value is consistent with that measured for Cu<sub>3</sub>P. 19 The addition of AgCl to In<sub>37</sub>P<sub>20</sub> MSCs leads to the growth of Ag 3d peaks, as seen in Figure 3B. As nanoscale Ag-P has not been successfully synthesized previously, there is no comparative XPS to examine. However, we see the growth of silver 3d peaks as more silver is added, indicating an increasing incorporation of silver into the material. Furthermore, these peaks closely correspond to the binding energy found for Ag<sub>2</sub>S.<sup>57</sup> Similarly, the addition of AuCl<sub>3</sub> to the In<sub>37</sub>P<sub>20</sub> MSC shows an increasing Au signal with more equivalents added, as shown in Figure 3C. In the Au sample, the initial binding energy of the  $4f_{7/2}$  peak is

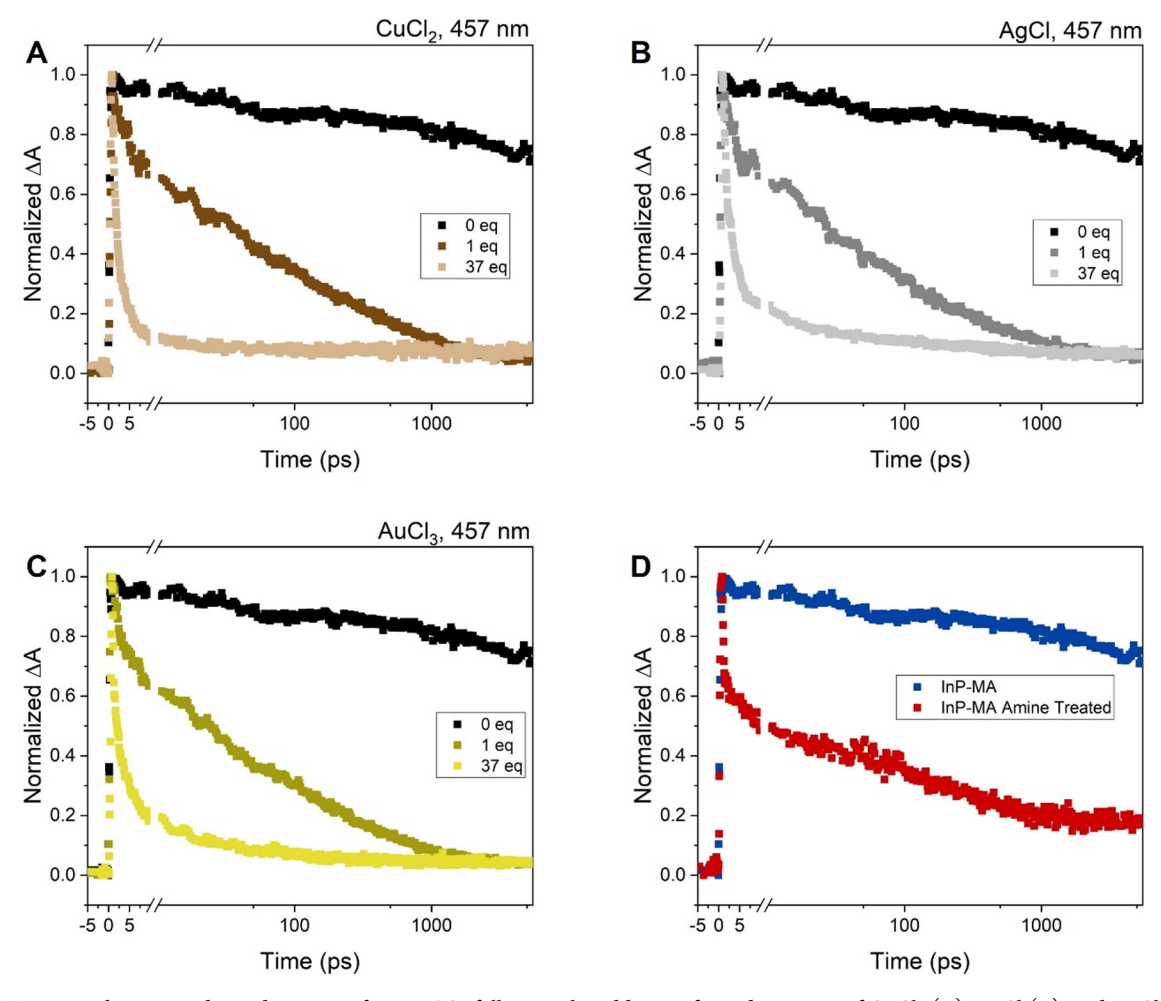


Figure 4. Transient absorption decay dynamics of InP MSCs following the addition of 1 and 37 equiv of  $CuCl_2$  (A), AgCl (B), and  $AuCl_3$  (C). (D) Transient absorption kinetics of myristate capped  $In_{37}P_{20}$  and amine-treated cluster.

84.2 eV, which is reminiscent of Au-amine complexes.<sup>58</sup> As more equivalents are added, the binding energy shifts to 84.5 eV, corresponding to Au in InP, 59 before shifting to higher binding energies, suggesting greater electronic interaction between the Au and P atoms in the lattice. For reference, XPS of as-synthesized In<sub>37</sub>P<sub>20</sub> MSCs shows In peaks characteristic of InP, centered at 444.7 eV, as shown in Figure 3D.60 After the introduction of any of these coinage metal dopants, the peaks begin to shift to higher binding energy, with shifts of over 1 eV, to 445.9 eV, highly reminiscent of  $InCl_3$  or  $In(O_2CR)_3$ . As such, we posit that many of the In ions have been exchanged out of the cluster core and remain instead as loosely associated molecular or surface-bound species. Upon adding 37 equiv of Cu, we see a complete loss of the In signal, suggesting complete cation exchange. These data correspond well with other forms of atomic elemental analysis, with inductively coupled plasma - optical emission spectrometry (ICP-OES) data showing little to no evidence of indium left in the core of the fully exchanged nanocrystals (Table S2).

As previous reports have shown, introducing coinage metals to InP quantum dots drastically affects their charge carrier lifetimes. 36,60,61 We turned to transient absorption spectroscopy to examine whether a similar phenomenon would occur with these smaller materials. The transient absorption spectra of cation-exchanged MSCs were strongly affected by increasing molar equivalents of coinage metal cations. In lightly doped

samples, a broadening that matches the change in the absorption profile is observed (Figure S9). Clusters doped with a single equivalent of coinage metal show a drastic reduction in both the bleach and photoinduced absorption lifetimes, as shown in Figure 4A-C, with lifetimes for Cu-, Ag-, and Au-doped clusters of 210, 150, and 120 ps, respectively. In contrast, the undoped clusters have lifetimes of 1550 ps, as shown in Figure 4D. This relatively long lifetime is attributable to the localization of the charge carriers in the distorted excited state of the InP MSC, analogous to molecular species. 62,63 The drastic differences in excited state lifetimes observed here could be attributed to the evolution of MSCs from a molecular-like species with highly localized frontier orbitals to one with a much more delocalized electronic structure as structural rearrangement occurs near the surface to alleviate strain.<sup>62</sup> Additional transient absorption studies show that the lifetime of the same cluster treated with amine is reduced but is longer than that of the doped species, as shown in the kinetic data in Figure 4D. The large number of new midgap states introduced upon doping, evident from the broadened absorption spectra in Figure 1, is expected to facilitate rapid nonradiative recombination, thus leading to shorter lifetimes. Interestingly, our pXRD data (Figure 2) suggest that the structure of the InP MSCs is maintained at low equivalents of dopant. Instead, we posit that the addition of our dopant solution causes a loss of indium carboxylate with concerted coordination of the dopant metal halide complex, followed by

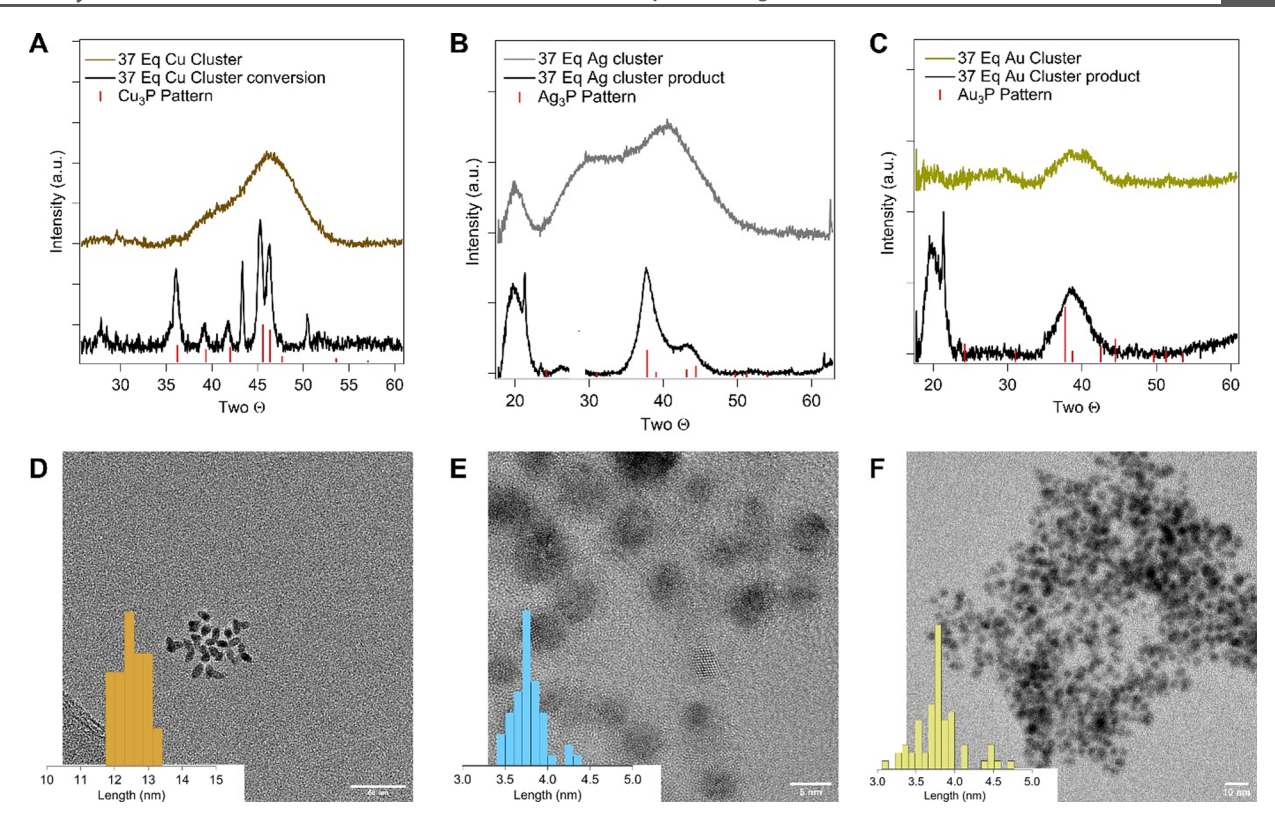


Figure 5. (A) pXRD of MSCs treated with 37 equiv of Cu before and after hot injection. The peak at 43 corresponds to forming a small fraction of large Cu nanocrystals. (B) pXRD of MSCs treated with 37 equiv of Ag before and after hot injection (the Si 111 peak at 28.4 has been removed from the analysis for clarity). (C) pXRD of MSCs treated with 37 equiv of Au before and after hot injection. (D) TEM of MSCs treated with 37 equiv of Cu after hot injection (scale bar is 50 nm). (E) TEM of MSCs treated with 37 equiv of Ag after hot injection (scale bar is 5 nm). (F) TEM of MSCs treated with 37 equiv of Au after hot injection (scale bar is 10 nm).

rearrangement of this new mixed carboxylate-halide ligand shell as the dopant migrates to the core, leading to a cluster with less highly localized frontier orbitals. This analysis is consistent with previous reports by our group detailing the liberation of indium carboxylates upon the addition of amine ligands as discussed previously. This mechanism is further supported by previous theoretical studies showing that the initial reactivity of InP increases with decreasing size and In—In separation and that doping aliovalent ions is more favorable following ligand removal. \$5,64,65

Upon addition of 37 equiv of coinage metal precursor, the original bleach and photoinduced absorption profile is eliminated. Instead, the TA signal is replaced by a rapid, broad photoinduced absorption feature, as seen in Figures S10 and 11, indicating that the new clusters have an excited state absorption coefficient greater than the ground state absorption coefficient at these wavelengths, similar to coinage metal chalcogenides. 66-68

Further interest in these coinage metal-containing clusters derives from their utility as single-source precursors for forming larger nanocrystals.  $^{2,69-71}$  After converting the  $\rm In_{37}P_{20}$  MSCs to coinage metal phosphide clusters, we examined whether these materials could be used to create larger nanocrystals. We hypothesized that a hot-injection synthesis could overcome the energic barrier keeping MSCs in their metastable state and allowing them to convert to larger, more stable nanocrystals. Indeed, upon injecting MSCs treated with one equivalent of copper into an ODE heated to 300  $^{\circ}{\rm C}$ , we obtain Cu+:InP quantum dots. This can be observed in Figure S11 by the broadened absorption profile along with

broad NIR luminescence, mirroring previously reported Cu<sup>+</sup>:InP systems. <sup>35,36,72</sup> Furthermore, these samples show highly similar diffraction patterns to undoped InP, suggesting that the zincblende InP lattice is retained (Figure S12).

However, using the fully cation-exchanged clusters yields different products. Upon conversion of the MSCs treated with 37 equiv of copper, the major product is  $Cu_{3-x}P$  nanocrystals, confirmed via pXRD analysis, as shown in Figure 5A. TEM analysis (Figure 5D) indicates the formation of larger (12.5  $\pm$ 0.5 nm) oblong nanocrystals. Hot injection of the MSCs treated with 37 equiv of silver leads to greater structural transformation of the cluster, with the pXRD in Figure 5B showing the formation of  $Ag_{3-x}P$  in the tetragonal phase. Excitingly, this is the first report of this material on the nanoscale to the best of our knowledge.<sup>73</sup> TEM analysis of these new Ag<sub>3-x</sub>P nanocrystals shows an average size of 3.8  $\pm$ 0.2 nm (Figure 5E), suggesting much less growth than that in the Cu-P system. Performing a hot-injection reaction of the MSCs treated with 37 equiv of Au with identical reaction parameters does not form nanocrystals of a new morphology. Instead, it grows in the cluster-based structure, as seen by the peak sharpening in the pXRD (Figure 5C) and growth to  $3.8 \pm$ 0.3 nm in size as seen via TEM (Figure 5F). Interestingly, we do not observe LSPR features in the NIR region of the absorption spectrum for any of these nanocrystals (Figure S13).

## EXPERIMENTAL METHODS

**Methods and Materials.** All glassware was dried in a 160 °C oven overnight prior to use. All reactions were run under an inert

**Chemistry of Materials** Article pubs.acs.org/cm

atmosphere of nitrogen using a glovebox or standard Schlenk line techniques. Indium(III) acetate (99.99%), myristic acid (99%), copper(II) chloride (≥98%), copper(I) chloride (97%), silver(I) chloride (99%), gold(III) chloride (99%), gold(I) chloride (99.9%), tributylphosphine (TBP), anhydrous acetonitrile, and anhydrous ethanol were purchased from Millipore-Sigma, stored in a nitrogen glovebox or desiccator, and used without further purification. Oleylamine, octadecene, and toluene were purchased from Millipore-Sigma, dried over CaH<sub>2</sub>, distilled, and stored over 4 Å sieves in a nitrogen glovebox.

Synthesis of InP MSCs. InP MSCs were synthesized according to previously established procedures from Gary et al. In brief, indium acetate and myristic acid were heated to 110 °C overnight under reduced pressure. Dry toluene was added to the backfilled reaction flask the next day and P(SiMe<sub>3</sub>)<sub>3</sub> in toluene was added. Cluster growth was allowed to proceed for 30 min. Purification was achieved via 4 successive cycles of precipitation/redissolution with toluene and acetonitrile as the solvent and antisolvent, respectively.

Cation Exchange Involving InP MSCs. Cation exchange was carried out at room temperature in an inert atmosphere glovebox. In a typical exchange reaction, ~10 mg of InP MSC was suspended in 1 mL of toluene and a solution of CuCl<sub>2</sub>, CuCl, AgCl, AuCl<sub>3</sub>, or AuCl solubilized in toluene and oleylamine (3:2 ratio) was added to the solution. Stock cation solutions were made at a concentration of 121 mM and added in quantities between 5  $\mu$ L (1 equiv) and 185  $\mu$ L (37 equiv) to the solution of InP MSCs and allowed to stir overnight. Cation-exchanged clusters were then purified via gel permeation chromatography as described in Shen et al.74

Conversion Reactions Involving Cation-Exchanged InP MSCs. Conversion reactions were carried out by suspending 10 mg of cation-exchanged clusters in 1 mL of octadecene, after which this solution was injected into a solution of 5 mL of a heated ODE at 300 °C. This reaction was allowed to proceed for 30 min at 300 °C. After the reaction was cooled, it was brought into an inert atmosphere glovebox and purified using 3 successive cycles of precipitation/ dissolution with toluene/ethanol as the solvent/antisolvent.

Characterization. UV-vis absorption spectroscopy was carried out on an Agilent Cary 5000 spectrophotometer. ICP data was collected on a Perkin Elmer Optima 8300 inductively coupled plasma - optical emission spectrophotometer. XPS was conducted on a Kratos AXIS Ultra DLD instrument located in the University of Washington Molecular Analysis Facility. The samples were drop-cast onto a silicon wafer from toluene in a N2 glovebox. Pass energy for survey spectra (to calculate composition) was 150 eV. Data point spacing was 1.0 eV per step for survey spectra and 0.4 eV per step for detailed spectra. Pass energy for high-resolution spectra was 50 eV, with a data point spacing of 0.065 eV. CasaXPS data analysis software was used to fit high-resolution spectra. Transient absorption measurements were performed using a HELIOS unit from Ultrafast Systems at the University of Washington's Molecular Analysis Facility. The pump wavelength was 386 nm and the power was measured as 200-500 uW. The probe white light was generated by using a CaF2 crystal. TEM images were collected on an FEI Tecnai G2 F20 microscope at 200 kV at the University of Washington Molecular Analysis Facility. TEM samples were prepared by spotting 5  $\mu$ L of a dilute solution of clusters or NCs dispersed in toluene onto an ultrathin carbon on a holey carbon support film purchased from Ted Pella. pXRD data were collected on a Bruker D8 Discover diffractometer with a Cu anode microfocus X-ray source and a Pilatus 100k large-area 2D detector. Samples were prepared by dissolving or suspending the sample in a minimal amount of toluene and repeatedly drop-casting 3  $\mu$ L of the solution onto a Si wafer to build up a thick film or layer of the sample. The beam for the measurement was collimated to a 1 mm beam diameter. Collection times were 360 s per step (5.5° step size). Raw diffraction data were processed using Bruker DIFFRAC.EVA software. For PDF analysis, MSC samples were first dried in an inert nitrogen atmosphere glovebox and sealed in quartz capillaries. X-ray total scattering data were collected on NSLS-II beamline 28-ID-1 at the Brookhaven National Laboratory. Sample scans consisted of 300 1-s exposures using 74.5 keV incident beam energy. Background

subtraction and transmission correction were applied to each scan. Sample transmission ranging from 67 to 84% was measured using a silicon photodiode with an impedance-amplifying circuit.

## CONCLUSIONS

We have demonstrated the room temperature conversion of  $In_{37}P_{20}$  MSCs into doped InP clusters and  $M_{3-x}P$  (M = Cu, Ag, Au) nanocrystals by exchange of indium using a coinage metal salt. We determined from a combination of absorption spectroscopy and pXRD data that the MSC core undergoes doping without significant structural changes upon adding 1 to 5 equiv of coinage metal. However, at 37 equiv of added coinage metal, we observe the complete transformation into new metal phosphide clusters with no evidence of remaining indium in the core as evidenced by XPS, ICP, and PDF analysis. Transient absorption spectroscopy of MSCs exposed to 1 equiv of coinage metal reactant suggests that removal of some excess surface In is required before transformation of the inorganic core can occur, while further exchange exhibits characteristics expected from the metallic character of coinage metal phosphides. Hot injection reactions of these new coinage metal phosphide clusters produce larger metal phosphide nanocrystals that reflect the cluster compositions. Notably, colloidal nanocrystals of Ag<sub>3-x</sub>P and Au<sub>3-x</sub>P have not been previously reported. This work illustrates that cation exchange can be used not only as a method to study structural transformations in MSCs but also as an approach to expand the library of MSCs that serve as intermediates in the formation of a variety of nanocrystals, including metastable or otherwise difficult to form species.

# ASSOCIATED CONTENT

# Supporting Information

The Supporting Information is available free of charge at https://pubs.acs.org/doi/10.1021/acs.chemmater.3c03258.

Supporting data and figures, including UV-vis spectra, XPS data, ICP-OES results, TEM images, and XRD data, can be found in the Supporting Information (PDF)

# AUTHOR INFORMATION

# **Corresponding Author**

Brandi M. Cossairt - Department of Chemistry, University of Washington, Seattle, Washington 98195-1700, United States; orcid.org/0000-0002-9891-3259;

Email: cossairt@uw.edu

### Authors

Forrest W. Eagle – Department of Chemistry, University of Washington, Seattle, Washington 98195-1700, United States Samantha Harvey - Department of Chemistry, University of Washington, Seattle, Washington 98195-1700, United States Helen Larson – Department of Chemistry, University of Washington, Seattle, Washington 98195-1700, United States Autumn Abbott - Department of Chemistry, University of Washington, Seattle, Washington 98195-1700, United States Dylan M. Ladd - Department of Materials Science and Engineering, University of Colorado, Boulder, Colorado 80309, United States; o orcid.org/0000-0002-9242-4382 Kelsey R. Levine - Department of Materials Science and

Engineering, University of Colorado, Boulder, Colorado 80309, United States

Michael F. Toney – Department of Materials Science and Engineering and Department of Chemical and Biological

Engineering, Renewable and Sustainable Energy Institute, University of Colorado, Boulder, Colorado 80309, United States; oocid.org/0000-0002-7513-1166

Daniel R. Gamelin — Department of Chemistry, University of Washington, Seattle, Washington 98195-1700, United States; orcid.org/0000-0003-2888-9916

Complete contact information is available at: https://pubs.acs.org/10.1021/acs.chemmater.3c03258

#### Notes

The authors declare no competing financial interest.

# ACKNOWLEDGMENTS

This research was supported by the U.S. National Science Foundation (NSF) through the UW Molecular Engineering Materials Center (MEM-C), a Materials Research Science and Engineering Center (Grant Nos. DMR-1719797 and DMR-2308979). The authors acknowledge the use of facilities and instrumentation supported by the U.S. National Science Foundation through the UW MEM-C (DMR-1719797 and DMR-2308979). Part of this work was conducted at the Molecular Analysis Facility, a National Nanotechnology Coordinated Infrastructure site at the University of Washington, which is supported, in part, by the National Science Foundation (Grant No. NNCI-1542101), the University of Washington, the Molecular Engineering and Sciences Institute, and the Clean Energy Institute. S.H. gratefully acknowledges fellowship support from the Department of Energy Office of Basic Sciences (Grant No. DE-SC0021232).

# REFERENCES

- (1) Cunningham, P. D.; Coropceanu, I.; Mulloy, K.; Cho, W.; Talapin, D. V. Quantized Reaction Pathways for Solution Synthesis of Colloidal ZnSe Nanostructures: A Connection between Clusters, Nanowires, and Two-Dimensional Nanoplatelets. *ACS Nano* **2020**, *14* (4), 3847–3857.
- (2) Gary, D. C.; Terban, M. W.; Billinge, S. J. L.; Cossairt, B. M. Two-Step Nucleation and Growth of InP Quantum Dots via Magic-Sized Cluster Intermediates. *Chem. Mater.* **2015**, 27 (4), 1432–1441.
- (3) Friedfeld, M. R.; Stein, J. L.; Cossairt, B. M. Main-Group-Semiconductor Cluster Molecules as Synthetic Intermediates to Nanostructures. *Inorg. Chem.* **2017**, *56* (15), 8689–8697.
- (4) Fenton, J. L.; Steimle, B. C.; Schaak, R. E. Tunable Intraparticle Frameworks for Creating Complex Heterostructured Nanoparticle Libraries. *Science* **2018**, *360* (6388), 513–517.
- (5) Steimle, B. C.; Fenton, J. L.; Schaak, R. E. Rational Construction of a Scalable Heterostructured Nanorod Megalibrary. *Science* **2020**, 367 (6476), 418–424.
- (6) Stone, D.; Koley, S.; Remennik, S.; Asor, L.; Panfil, Y. E.; Naor, T.; Banin, U. Luminescent Anisotropic Wurtzite InP Nanocrystals. *Nano Lett.* **2021**, *21* (23), 10032–10039.
- (7) De Trizio, L.; Gaspari, R.; Bertoni, G.; Kriegel, I.; Moretti, L.; Scotognella, F.; Maserati, L.; Zhang, Y.; Messina, G. C.; Prato, M.; Marras, S.; Cavalli, A.; Manna, L. Cu <sub>3-x</sub> P Nanocrystals as a Material Platform for Near-Infrared Plasmonics and Cation Exchange Reactions. *Chem. Mater.* **2015**, *27* (3), 1120–1128.
- (8) Beberwyck, B. J.; Alivisatos, A. P. Ion Exchange Synthesis of III—V Nanocrystals. J. Am. Chem. Soc. 2012, 134 (49), 19977–19980.
- (9) White, S. L.; Banerjee, P.; Chakraborty, I.; Jain, P. K. Ion Exchange Transformation of Magic-Sized Clusters. *Chem. Mater.* **2016**, 28 (22), 8391–8398.
- (10) Stein, J. L.; Steimle, M. I.; Terban, M. W.; Petrone, A.; Billinge, S. J. L.; Li, X.; Cossairt, B. M. Cation Exchange Induced Transformation of InP Magic-Sized Clusters. *Chem. Mater.* **2017**, 29 (18), 7984–7992.

- (11) He, L.; Luan, C.; Liu, S.; Chen, M.; Rowell, N.; Wang, Z.; Li, Y.; Zhang, C.; Lu, J.; Zhang, M.; Liang, B.; Yu, K. Transformations of Magic-Size Clusters via Precursor Compound Cation Exchange at Room Temperature. *J. Am. Chem. Soc.* **2022**, *144* (41), 19060–19069.
- (12) Muckel, F.; Yang, J.; Lorenz, S.; Baek, W.; Chang, H.; Hyeon, T.; Bacher, G.; Fainblat, R. Digital Doping in Magic-Sized CdSe Clusters. ACS Nano 2016, 10 (7), 7135–7141.
- (13) Yang, J.; Fainblat, R.; Kwon, S. G.; Muckel, F.; Yu, J. H.; Terlinden, H.; Kim, B. H.; Iavarone, D.; Choi, M. K.; Kim, I. Y.; Park, I.; Hong, H.-K.; Lee, J.; Son, J. S.; Lee, Z.; Kang, K.; Hwang, S.-J.; Bacher, G.; Hyeon, T. Route to the Smallest Doped Semiconductor: Mn2+-Doped (CdSe)13 Clusters. *J. Am. Chem. Soc.* **2015**, *137* (40), 12776–12779.
- (14) Pittala, S.; Mortelliti, M. J.; Kato, F.; Kittilstved, K. R. Substitution of Co2+ Ions into CdS-Based Molecular Clusters. *Chem. Commun.* **2015**, *51* (96), 17096–17099.
- (15) Eilers, J.; Groeneveld, E.; de Mello Donegá, C.; Meijerink, A. Optical Properties of Mn-Doped ZnTe Magic Size Nanocrystals. *J. Phys. Chem. Lett.* **2012**, 3 (12), 1663–1667.
- (16) Fainblat, R.; Barrows, C. J.; Gamelin, D. R. Single Magnetic Impurities in Colloidal Quantum Dots and Magic-Size Clusters. *Chem. Mater.* **2017**, 29 (19), 8023–8036.
- (17) Lin, J.; Zhang, Q.; Wang, L.; Liu, X.; Yan, W.; Wu, T.; Bu, X.; Feng, P. Atomically Precise Doping of Monomanganese Ion into Coreless Supertetrahedral Chalcogenide Nanocluster Inducing Unusual Red Shift in Mn2+ Emission. *J. Am. Chem. Soc.* **2014**, *136* (12), 4769–4779.
- (18) Friedfeld, M. R.; Stein, J. L.; Johnson, D. A.; Park, N.; Henry, N. A.; Enright, M. J.; Mocatta, D.; Cossairt, B. M. Effects of Zn2+ and Ga3+ Doping on the Quantum Yield of Cluster-Derived InP Quantum Dots. J. Chem. Phys. 2019, 151 (19), 194702.
- (19) Rivest, J. B.; Jain, P. K. Cation Exchange on the Nanoscale: An Emerging Technique for New Material Synthesis, Device Fabrication, and Chemical Sensing. *Chem. Soc. Rev.* **2013**, *42* (1), 89–96.
- (20) Manna, G.; Bose, R.; Pradhan, N. Semiconducting and Plasmonic Copper Phosphide Platelets. *Angew. Chem., Int. Ed.* **2013**, 52 (26), 6762–6766.
- (21) Rachkov, A. G.; Schimpf, A. M. Colloidal Synthesis of Tunable Copper Phosphide Nanocrystals. *Chem. Mater.* **2021**, 33 (4), 1394–1406
- (22) Bertoni, G.; Ramasse, Q.; Brescia, R.; De Trizio, L.; De Donato, F.; Manna, L. Direct Quantification of Cu Vacancies and Spatial Localization of Surface Plasmon Resonances in Copper Phosphide Nanocrystals. ACS Mater. Lett. 2019, 1 (6), 665–670.
- (23) Tian, J.; Liu, Q.; Cheng, N.; Asiri, A. M.; Sun, X. Self-Supported Cu3P Nanowire Arrays as an Integrated High-Performance Three-Dimensional Cathode for Generating Hydrogen from Water. *Angew. Chem., Int. Ed.* **2014**, *53* (36), 9577–9581.
- (24) Zhou, X.; Zhou, X.; Liu, L.; Chen, H.; Hu, X.; Qian, J.; Huang, D.; Zhang, B.; Tang, J. Self-Supported Cu <sub>3</sub> P Nanowire Electrode as an Efficient Electrocatalyst for the Oxygen Evolution Reaction. *RSC Adv.* **2021**, *11* (54), 34137–34143.
- (25) Laursen, A. B.; Calvinho, K. U. D.; Goetjen, T. A.; Yap, K. M. K.; Hwang, S.; Yang, H.; Garfunkel, E.; Dismukes, G. C. CO2 Electro-Reduction on Cu3P: Role of Cu(I) Oxidation State and Surface Facet Structure in C1-Formate Production and H2 Selectivity. *Electrochim. Acta* 2021, 391, No. 138889.
- (26) Downes, C. A.; Libretto, N. J.; Harman-Ware, A. E.; Happs, R. M.; Ruddy, D. A.; Baddour, F. G.; Ferrell, J. R., III; Habas, S. E.; Schaidle, J. A. Electrocatalytic CO2 Reduction over Cu3P Nanoparticles Generated via a Molecular Precursor Route. *ACS Appl. Energy Mater.* **2020**, 3 (11), 10435–10446.
- (27) Carenco, S.; Florea, I.; Ersen, O.; Boissière, C.; Mézailles, N.; Sanchez, C. Towards Nanoscaled Gold Phosphides: Surface Passivation and Growth of Composite Nanostructures. *New J. Chem.* **2013**, 37 (4), 1231–1237.
- (28) Okamoto, H.; Massalski, T. B. The Au–P (Gold-Phosphorus) System. *Bulletin of Alloy Phase Diagrams* **1984**, 5 (5), 490–491.

- (29) Sweeney, C. M.; Stamm, K. L.; Brock, S. L. On the Feasibility of Phosphide Generation from Phosphate Reduction: The Case of Rh, Ir, and Ag. *J. Alloys Compd.* **2008**, 448 (1), 122–127.
- (30) Li, H.; Wen, P.; Itanze, D. S.; Hood, Z. D.; Ma, X.; Kim, M.; Adhikari, S.; Lu, C.; Dun, C.; Chi, M.; Qiu, Y.; Geyer, S. M. RETRACTED ARTICLE: Colloidal Silver Diphosphide (AgP2) Nanocrystals as Low Overpotential Catalysts for CO2 Reduction to Tunable Syngas. *Nature Commun.* **2019**, *10* (1), 5724.
- (31) Vaughey, J. T.; Fransson, L.; Swinger, H. A.; Edström, K.; Thackeray, M. M. Alternative Anode Materials for Lithium-Ion Batteries: A Study of Ag3Sb. *J. Power Sources* **2003**, *119–121*, 64–68.
- (32) Okamoto, H.; Schlesinger, M. E.; Mueller, E. M., Eds. Ag (Silver) Binary Alloy Phase Diagrams. In Alloy Phase Diagrams. 2016.
- (33) Cipriani, C.; Corazza, M.; Mazzetti, G. Reinvestigation of Natural Silver Antimonides. *ejm* **1996**, 8 (6), 1347–1350.
- (34) Henkes, A. E.; Vasquez, Y.; Schaak, R. E. Converting Metals into Phosphides: A General Strategy for the Synthesis of Metal Phosphide Nanocrystals. *J. Am. Chem. Soc.* **2007**, *129* (7), 1896–1897.
- (35) Knowles, K. E.; Hartstein, K. H.; Kilburn, T. B.; Marchioro, A.; Nelson, H. D.; Whitham, P. J.; Gamelin, D. R. Luminescent Colloidal Semiconductor Nanocrystals Containing Copper: Synthesis, Photophysics, and Applications. *Chem. Rev.* **2016**, *116* (18), 10820–10851.
- (36) Knowles, K. E.; Nelson, H. D.; Kilburn, T. B.; Gamelin, D. R. Singlet—Triplet Splittings in the Luminescent Excited States of Colloidal Cu+:CdSe, Cu+:InP, and CuInS2 Nanocrystals: Charge-Transfer Configurations and Self-Trapped Excitons. *J. Am. Chem. Soc.* 2015, 137 (40), 13138–13147.
- (37) Nelson, H. D.; Li, X.; Gamelin, D. R. Computational Studies of the Electronic Structures of Copper-Doped CdSe Nanocrystals: Oxidation States, Jahn—Teller Distortions, Vibronic Bandshapes, and Singlet—Triplet Splittings. *J. Phys. Chem. C* **2016**, 120 (10), 5714—5723.
- (38) Gary, D. C.; Flowers, S. E.; Kaminsky, W.; Petrone, A.; Li, X.; Cossairt, B. M. Single-Crystal and Electronic Structure of a 1.3 Nm Indium Phosphide Nanocluster. *J. Am. Chem. Soc.* **2016**, *138* (5), 1510–1513.
- (39) Bhuse, V. M.; Hankare, P. P.; Garadkar, K. M.; Khomane, A. S. A Simple, Convenient, Low Temperature Route to Grow Polycrystal-line Copper Selenide Thin Films. *Mater. Chem. Phys.* **2003**, *80* (1), 82–88.
- (40) Liu, Y.; Liu, M.; Swihart, M. T. Plasmonic Copper Sulfide-Based Materials: A Brief Introduction to Their Synthesis, Doping, Alloying, and Applications. *J. Phys. Chem. C* **2017**, *121* (25), 13435–13447.
- (41) White, S. L.; Banerjee, P.; Jain, P. K. Liquid-like Cationic Sub-Lattice in Copper Selenide Clusters. *Nature Commun.* **2017**, 8 (1), 14514.
- (42) Liu, Z.; Zhong, Y.; Shafei, I.; Jeong, S.; Wang, L.; Nguyen, H. T.; Sun, C.-J.; Li, T.; Chen, J.; Chen, L.; Losovyj, Y.; Gao, X.; Ma, W.; Ye, X. Broadband Tunable Mid-Infrared Plasmon Resonances in Cadmium Oxide Nanocrystals Induced by Size-Dependent Nonstoichiometry. *Nano Lett.* **2020**, *20* (4), 2821–2828.
- (43) Schimpf, A. M.; Thakkar, N.; Gunthardt, C. E.; Masiello, D. J.; Gamelin, D. R. Charge-Tunable Quantum Plasmons in Colloidal Semiconductor Nanocrystals. *ACS Nano* **2014**, 8 (1), 1065–1072.
- (44) Jharimune, S.; Sathe, A. A.; Rioux, R. M. Thermochemical Measurements of Cation Exchange in CdSe Nanocrystals Using Isothermal Titration Calorimetry. *Nano Lett.* **2018**, *18* (11), 6795–6803
- (45) Hafiz, S. B.; Scimeca, M. R.; Zhao, P.; Paredes, I. J.; Sahu, A.; Ko, D.-K. Silver Selenide Colloidal Quantum Dots for Mid-Wavelength Infrared Photodetection. *ACS Appl. Nano Mater.* **2019**, 2 (3), 1631–1636.
- (46) León-Velázquez, M. S.; Irizarry, R.; Castro-Rosario, M. E. Nucleation and Growth of Silver Sulfide Nanoparticles. *J. Phys. Chem.* C **2010**, *114* (13), 5839–5849.
- (47) Akamatsu, K.; Takei, S.; Mizuhata, M.; Kajinami, A.; Deki, S.; Takeoka, S.; Fujii, M.; Hayashi, S.; Yamamoto, K. Preparation and

- Characterization of Polymer Thin Films Containing Silver and Silver Sulfide Nanoparticles. *Thin Solid Films* **2000**, 359 (1), 55–60.
- (48) Mourdikoudis, S.; Liz-Marzán, L. M. Oleylamine in Nanoparticle Synthesis. *Chem. Mater.* **2013**, 25 (9), 1465–1476.
- (49) Gary, D. C.; Petrone, A.; Li, X.; Cossairt, B. M. Investigating the Role of Amine in InP Nanocrystal Synthesis: Destabilizing Cluster Intermediates by Z-Type Ligand Displacement. *Chem. Commun.* **2017**, 53 (1), 161–164.
- (50) Anderson, N. C.; Hendricks, M. P.; Choi, J. J.; Owen, J. S. Ligand Exchange and the Stoichiometry of Metal Chalcogenide Nanocrystals: Spectroscopic Observation of Facile Metal-Carboxylate Displacement and Binding. *J. Am. Chem. Soc.* **2013**, *135* (49), 18536–18548.
- (51) Materials Data on Cu3P by Materials Project; mp-7463; Lawrence Berkeley National Lab. (LBNL): Berkeley, CA (United States). LBNL Materials Project, 2020.
- (52) Materials Data on PAu3 by Materials Project; mp-1186369; Lawrence Berkeley National Lab. (LBNL): Berkeley, CA (United States). LBNL Materials Project, 2020.
- (53) White, S. L.; Smith, J. G.; Behl, M.; Jain, P. K. Co-Operativity in a Nanocrystalline Solid-State Transition. *Nature Commun.* **2013**, *4* (1), 2933.
- (54) Yao, Y.; Lynch, R.; Robinson, R. D. Mass Spectroscopy Study of the Intermediate Magic-Size Cluster Species during Cooperative Cation Exchange. *J. Chem. Phys.* **2023**, *159* (1), No. 014704.
- (55) Taylor, M. G.; Kulik, H. J. Mapping the Origins of Surface- and Chemistry-Dependent Doping Trends in III–V Quantum Dots with Density Functional Theory. *Chem. Mater.* **2021**, 33 (17), 7113–7123.
- (56) Zhang, X.; Kim, D.; Guo, X.; Zhu, Y.; Lee, L. Y. S. Impacts of Boron Doping on the Atomic Structure, Stability, and Photocatalytic Activity of Cu3P Nanocrystals. *Appl. Catal., B* **2021**, 298, No. 120515.
- (57) Chowdari, B. V. R.; Mok, K. F.; Xie, J. M.; Gopalakrishnan, R. Spectroscopic and Electrical Studies of Silver Sulfophosphate Glasses. *J. Non-Cryst. Sol.* **1993**, *160* (1), 73–81.
- (58) Kitagawa, H.; Kojima, N.; Nakajima, T. Studies of Mixed-Valence States in Three-Dimensional Halogen-Bridged Gold Compounds, Cs2AuIAuIIIX6, (X = Cl, Br or I). Part 2. X-Ray Photoelectron Spectroscopic Study. *Dalton Trans.* **1991**, *11*, 3121–3125.
- (59) Wang, X.; Fei, Y.; Li, W.; Yi, L.; Feng, B.; Pan, Y.; Hu, W.; Li, C. M. Gold-Incorporated Cobalt Phosphide Nanoparticles on Nitrogen-Doped Carbon for Enhanced Hydrogen Evolution Electrocatalysis. ACS Appl. Mater. Interfaces 2020, 12 (14), 16548–16556.
- (60) Tao, Y.; Yelon, A.; Sacher, E.; Lu, Z. H.; Graham, M. J. Spassivated InP (100)-(1  $\times$  1) Surface Prepared by a Wet Chemical Process. *Appl. Phys. Lett.* **1992**, 60 (21), 2669–2671.
- (61) Freeland, B. H.; Habeeb, J. J.; Tuck, D. G. Coordination Compounds of Indium. Part XXXIII. X-Ray Photoelectron Spectroscopy of Neutral and Anionic Indium Halide Species. *Can. J. Chem.* 1977, 55 (9), 1527–1532.
- (62) Kwon, Y.; Oh, J.; Lee, E.; Lee, S. H.; Agnes, A.; Bang, G.; Kim, J.; Kim, D.; Kim, S. Evolution from Unimolecular to Colloidal-Quantum-Dot-like Character in Chlorine or Zinc Incorporated InP Magic Size Clusters. *Nature Commun.* **2020**, *11* (1), 3127.
- (63) Okuda, Y.; Tsurumaki, E.; Oh, J.; Sung, J.; Kim, D.; Osuka, A. A Directly Fused Subporphyrin Dimer with a Wavelike Structure. *Angew. Chem., Int. Ed.* **2016**, 55 (32), 9212–9215.
- (64) Zhao, Q.; Kulik, H. J. Electronic Structure Origins of Surface-Dependent Growth in III–V Quantum Dots. *Chem. Mater.* **2018**, *30* (20), 7154–7165.
- (65) Shim, D.; Kang, J. Enhanced Reactivity of Magic-Sized Inorganic Clusters by Engineering the Surface Ligand Networks. *Chem. Mater.* **2023**, 35 (2), 700–708.
- (66) Zhang, F.; Chen, K.; Jiang, X.; Wang, Y.; Ge, Y.; Wu, L.; Xu, S.; Bao, Q.; Zhang, H. Nonlinear Optical Absorption and Ultrafast Carrier Dynamics of Copper Antimony Sulfide Semiconductor Nanocrystals. *J. Mater. Chem. C* **2018**, *6* (33), 8977–8983.

- (67) Shi, G.; He, C.; Li, Y.; Zou, R.; Zhang, X.; Wang, Y.; Yang, K.; Song, Y.; Wang, C. H. Excited-State Nonlinearity Measurements of ZnPcBr<sub>4</sub>/DMSO. *J. Opt. Soc. Am. B, JOSAB* **2009**, 26 (4), 754–761. (68) Kriegel, I.; Jiang, C.; Rodríguez-Fernández, J.; Schaller, R. D.; Talapin, D. V.; da Como, E.; Feldmann, J. Tuning the Excitonic and Plasmonic Properties of Copper Chalcogenide Nanocrystals. *J. Am. Chem. Soc.* **2012**, 134 (3), 1583–1590.
- (69) Wang, Y.; Zhang, Y.; Wang, F.; Giblin, D. E.; Hoy, J.; Rohrs, H. W.; Loomis, R. A.; Buhro, W. E. The Magic-Size Nanocluster (CdSe)34 as a Low-Temperature Nucleant for Cadmium Selenide Nanocrystals; Room-Temperature Growth of Crystalline Quantum Platelets. *Chem. Mater.* **2014**, *26* (7), 2233–2243.
- (70) Cumberland, S. L.; Hanif, K. M.; Javier, A.; Khitrov, G. A.; Strouse, G. F.; Woessner, S. M.; Yun, C. S. Inorganic Clusters as Single-Source Precursors for Preparation of CdSe, ZnSe, and CdSe/ZnS Nanomaterials. *Chem. Mater.* **2002**, *14* (4), 1576–1584.
- (71) Li, L.; Zhang, J.; Zhang, M.; Rowell, N.; Zhang, C.; Wang, S.; Lu, J.; Fan, H.; Huang, W.; Chen, X.; Yu, K. Fragmentation of Magic-Size Cluster Precursor Compounds into Ultrasmall CdS Quantum Dots with Enhanced Particle Yield at Low Temperatures. *Angew. Chem., Int. Ed.* **2020**, 132 (29), 12111–12119.
- (72) Mundy, M. E.; Eagle, F. W.; Hughes, K. E.; Gamelin, D. R.; Cossairt, B. M. Synthesis and Spectroscopy of Emissive, Surface-Modified, Copper-Doped Indium Phosphide Nanocrystals. *ACS Materials Lett.* **2020**, *2* (6), 576–581.
- (73) Materials Data on Ag3P by Materials Project; mp-985295; Lawrence Berkeley National Lab. (LBNL): Berkeley, CA (United States). LBNL Materials Project, 2020.
- (74) Shen, Y.; Roberge, A.; Tan, R.; Gee, M. Y.; Gary, D. C.; Huang, Y.; Blom, D. A.; Benicewicz, B. C.; Cossairt, B. M.; Greytak, A. B. Gel Permeation Chromatography as a Multifunctional Processor for Nanocrystal Purification and On-Column Ligand Exchange Chemistry. *Chem. Sci.* **2016**, *7* (9), 5671–5679.